Research Article

# Characterization and Evaluation of Mechanical Properties of Al-Zn Based Hybrid Metal Matrix Composites

Kodigarahalli Somashekara Madhu*, Channarayapattana Venkataramaiah Venkatesh, Ballupete Nagaraju Sharath and Sathyanarayana Karthik

Department of Mechanical Engineering, Malnad College of Engineering, Hassan, Visvesvaraya Technological University, Belagavi, Karnataka, India

* Corresponding author. E-mail: mks@mcehassan.ac.in

**Abstract**

Hybrid aluminium matrix composites are preferred for structural applications due to their tailored material properties. In the current study, aluminium-7029 alloy with boron carbide (5, 10, and 15 wt%) and a constant weight percentage of graphite (5 wt%) were produced by the stir casting route. Scanning Electron Microscope and X-Ray Diffraction were used to characterize the composites. The cast alloy and hybrid composites were evaluated for physical (density and porosity) and mechanical (hardness, tensile, compressive and impact) properties by experimental and statistical methods. The porosity of the cast samples was minimal (<5%) and the hybrid composite weight decreased (2.4%) with the increase of reinforcements as revealed by the density test. Al7029/15wt%B$_4$C/5wt%Gr (sample C3) hybrid composite hardness (126 BHN) and compressive strength (586.841 MPa) were found to be the best to get the better property with more reinforcement. Tensile (253.455 MPa) and impact strength (7 J) were the highest for the Al7029/5wt%B$_4$C/5wt%Gr (sample C1) hybrid composite. Results obtained by a regression model developed using MINITAB were in good agreement with experimental values. The additions of B$_4$C and Gr were found to improve mechanical properties significantly, as confirmed by analysis of variance.

**Keywords**: Al7029, Boron carbide, Graphite, Mechanical properties, Statistical method

## 1 Introduction

Composites can be used in different ways in the aerospace and automotive industries because they have unique properties, especially the. Aluminium alloys in the 7-xxx series [1]. It is used in structural applications because of its lightweight and better properties, such as a high strength-to-weight ratio [1], [2]. By combining appropriate matrix, reinforcement, and processing techniques, the characteristics of Al7029 can be adapted to the needs of various industrial applications. Efforts have recently been undertaken to build composites with hard reinforcements, such as boron carbide (B$_4$C), silicon carbide (SiC), tungsten carbide (WC), graphite (Gr), etc., In the current scenario, most automotive structural and engine components are replaced by lightweight, high-strength aluminium metal matrix composites (AMMCs) [3]–[5]. Aluminium alloy reinforced with ceramic particles has been shown to have improved mechanical properties. B$_4$C enhances tensile, impact, and toughness properties, as well as interface bonding with the aluminium matrix, and Gr reduces the composite wear rate due to its self-lubricating capabilities. The most widely used industrial method for creating aluminium-based composites is stir casting due to its suitability for mass production and low cost [6]–[10]. Tungsten carbide (WC), fly ash (FA), B$_4$C and coconut shell fly ash (CSFA) were added to fabricate Al7xxx based hybrid composites. Results revealed that the composite possessed the higher hardness (94.4–169.5 BHN) and the better ultimate tensile strength (UTS) (233.33 MPa)

than the base alloy. Scanning Electron Microscope (SEM) micrographs reveal that reinforced particles act as barriers to material fracture [2], [11].

The Al356 based hybrid composites were fabricated by stir casting with the addition of Gr and $B_4C$. Test results revealed an increase in hardness, which resulted in a decrease in ductility. The density of the composite was found to be reduced by about 20% when compared with the base alloy [12]. The fractography results show that the $3\%h\text{-}BN/6\%ZrO_2$ composite has the highest hardness (92 BHN) and the maximum ultimate strength (187 MPa) with the enhanced wear rate [13]. The Al6061/SiC/Gr composite tensile strength increased (192 MPa) by 22% with a decrease in density of 7% compared to the Al6061/SiC composite. SEM found that the hybrid composite's properties were improved because it had more SiC particles [14].

Metal composites are being investigated for the optimization of data received from mechanical properties and corrosion tests carried out using standard testing methodologies [15], [16]. The flexural strength of $Al6061/2\%SiC/2\%B_4C$ was found to be high, along with tensile strength (128 MPa) and hardness (45.8 BHN). The reduced ductility, as confirmed by SEM results, is due to the increase of ceramic reinforcements [17]. The reinforcement effect and corrosion behavior of hybrid metal composites using the ASTM standard testing method for tensile and hardness were evaluated and found to have increased reinforcement as a direct effect on mechanical properties [18], [19].

Physical and mechanical properties of the $Al356.1/B_4C$ composite at temperatures of 800 ºC and 1000 ºC were found. With an increasing $B_4C$ weight percentage, the density of the composite decreased and the porosity increased. At 15% wt% $B_4C$, ultimate porosity was found to be higher. At 15 wt% $B_4C$, the UTS (211MPa) and hardness (94 BHN) were found to be the highest, due to particle strengthening at higher temperatures. The test results were validated by an artificial neural network [20]. An experimental and factorial design approach was used to find the micro hardness, tensile, and compression properties. The hardness of the hybrid composite enhanced by $B_4C$ particle addition, $Al7075/5\%B_4C/5\%RHA$ composite compressive strength (563 MPa), and Al7075 alloy with 5 wt% $B_4C$ tensile strength were higher. The presence of increased $B_4C$ particle reinforcement was the cause of the improved mechanical properties and

was confirmed by SEM [21]. The addition of more Gr (2–12 wt%) particles to the Al6351 alloy reduced its tensile and hardness. This was due to the brittle nature and improper distribution of Gr particles in the matrix, as confirmed by SEM micrographs [22]. Nano-sized $B_4C$ (3–6 wt%) was found to affect the mechanical properties of Al7075 alloy. The hardness, compressive, and tensile strength of the composite were found to be higher at 6 wt% $B_4C$ due to a decrease in strain rate [23].

In the present work, aluminium alloy (Al-7029), $B_4C$, and Gr hybrid composites were fabricated using conventional stir casting. In the view of lightweight structural applications, $B_4C$ and Gr particles are chosen. Since their densities are the same, and with enhanced strength, they can decrease the weight of the composite. The prepared composites were evaluated for physical and mechanical properties. Both experimental and statistical approaches were employed for correlating the results. The composite microstructures, elements presence and material phase were studied using SEM and X-ray diffraction (XRD).

## 2 Materials and Methods

### 2.1 *Raw material*

The matrix and reinforcing material make up the hybrid MMCs (HMMCs). As matrix material, Al7029 (Supplier: Fenfe Metallurgicals, India) is used and, as reinforcing materials, $B_4C$ (Supplier: Speedfam, India) and Gr (Supplier: Graphite India, India) are selected. The chemical composition of the Al7029 alloy is indicated in Table 1, and the material composition is indicated in Table 2. The Al7029 hybrid composites were produced with commercially available boron carbide and graphite reinforcements (a particle size average of 50 µm).

### 2.2 *Fabrication of hybrid composite*

In a 5-kW electrical furnace, the stir casting method was employed to create hybrid $Al7029/B_4C/Gr$ composites. Al7029 was kept in a graphite crucible for 90 min at a temperature between 600 and 700 ºC. As the Al7029 ingot material reached the molten stage, Mg (3%) was added to facilitate wettability within the matrix and reinforcement. To obtain the uniform distribution of $B_4C$ particulate (50 µm) in the Al7029
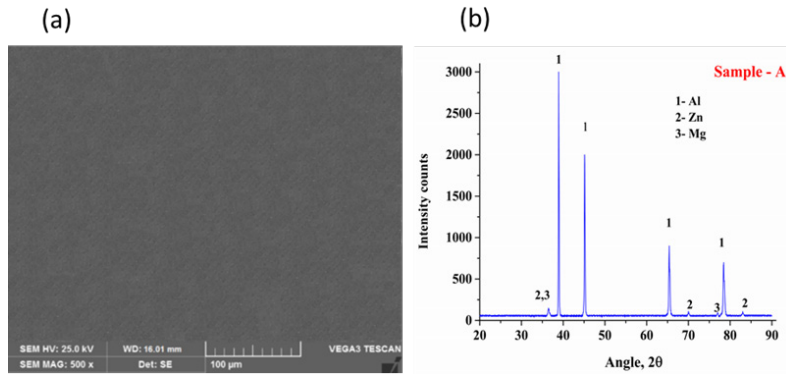
**Figure 1**: Characterization of sample A, (a) SEM micrograph, (b) XRD pattern.
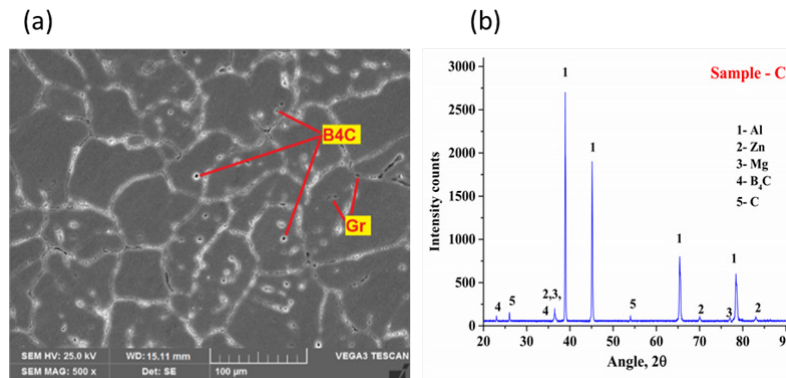


**Figure 2**: Characterization of sample C1, (a) SEM micrograph, (b) SEM micrograph.

matrix, $B_4C$ was pre-heated to 500 ºC and poured into the molten metal and stirred at a constant speed of 150 rpm for 15–20 min. Pre-heated graphite (5 wt%) was added to the pre-mixed molten Al7029 with $B_4C$. Stirring is continued for another 10–15 min to ensure that Gr and the molten metal is well mixed. To reduce casting defects, hexachloroethane is used. Hot molten metal is transferred to a pre-heated die and allowed to solidify at room temperature [7], [10].

**Table 1**: Chemical composition of Al7029 alloy

| Element | Mass Fraction % |
|---------|-----------------|
| Si | 0.1 |
| Fe | 0.12 |
| Cu | 0.5–0.9 |
| Mn | 0.03 |
| Mg | 1.3–2 |
| Zn | 4.2–5.2 |
| Ti | 0.05 |
| V | 0.05 |
| Al | Bal |

**Table 2**: Material composition in weight percentage

| Sample | Al7029 | $B_4C$ | Gr |
|--------|--------|--------|-----|
| A | 100 | 0 | 0 |
| C1 | 90 | 5 | 5 |
| C2 | 85 | 10 | 5 |
| C3 | 80 | 15 | 5 |

**2.3 SEM and XRD analysis**

SEM and XRD micrographs of Al7029 and hybrid Al7029 composites are shown in Figures 1–4. The $B_4C$ and Gr particles are uniformly dispersed throughout the Al7029 matrix, which are noticed through SEM micrographs [Figures 1(a), 2(a), 3(a), and 4(a)]. In grain boundary regions, $B_4C$ particles are caught in dendritic geometrical entrapment, which increase the bonding between the matrix and the reinforcement [10]. Also, both reinforcements act as impediments to dislocations in the boundary region [17]. Figures 1(b), 2(b), 3(b), and 4(b) from the XRD analysis show
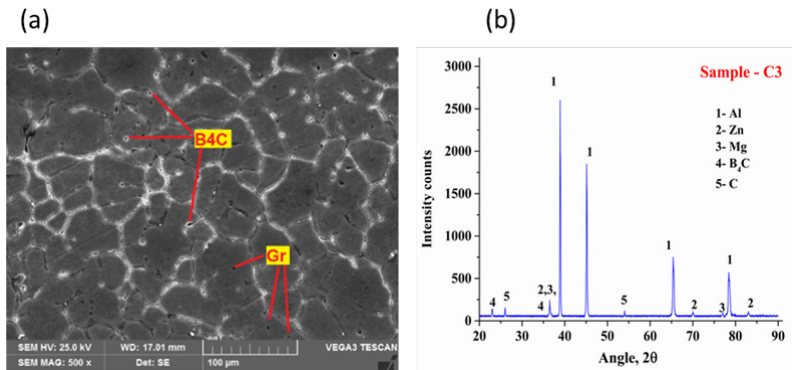
**Figure 3**: Characterization of sample C2, (a) SEM micrograph, (b) XRD pattern.
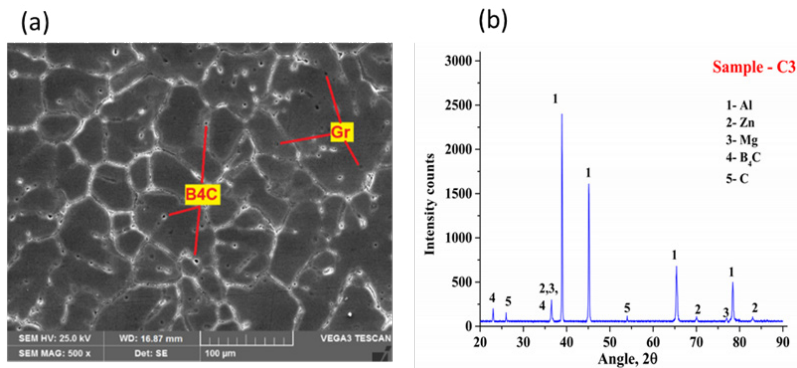


**Figure 4**: Characterization of sample C3, (a) SEM micrograph, (b) XRD pattern.

an increase in peak height at the higher $B_4C$ weight percentages. An aluminium phase and the elements Zn and Mg can be seen at peaks of 38°, 45°, 65°, and 78°.

The presence of graphite is indicated by an X-ray intensity peak of 26° and 54°. The X-ray intensity of $B_4C$ particles ranges from 23° to 36° [24], [25]. Uniform particle distribution noticed from SEM and XRD graphs confirms elemental presence with no phase change within the matrix, which would enhance the mechanical properties of HMMCs.

### 2.4 Density and porosity test

The density was calculated using the well-known Archimedes principle: knowing the mass and volume of an object allows calculating the density. Porosity, or void fraction, is a measure of the voids in a material and is a fraction of the volume of voids over the total volume, between 0 and 1, or as a percentage between 0% and 100%.

### 2.5 Micro hardness test

The hardness of HMMCs is measured using the Brinell hardness testing method (Make: Mechatronic Systems QNESS 60M EVO). The ASTM standard for hardness testing used was E-10. The Brinell method measures the permanent depth of indentation produced by applying a load of 240 kgf for a time period of 30 s on AMMCs. Five different readings were taken on the same sample, and an average value was taken [26]–[30].

### 2.6 Tensile test

The cast samples were machined according to ASTM standard E-8 and tensile tests were performed using a universal testing machine (UTM) with a load cell capacity of 0–50 kN (Make: BiSS Microsystems: UT-02-005). Cross head speed moved upwards at a constant rate of $8 \times 10^{-4}$ m/s. For each composition, five
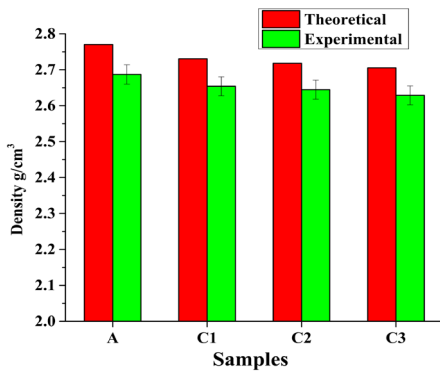
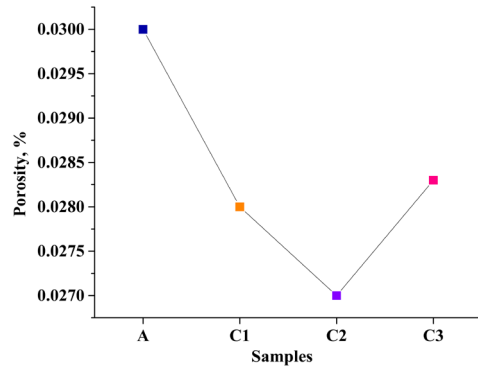**Figure 5**: Theoretical vs Experimental density.



**Figure 6**: Porosity of cast samples.

samples were tested, and the average was considered for the study.

### 2.7 *Compression test*

The compression test was carried out in accordance with ASTM standard E9. The compression test is performed on a cylindrical object using a universal testing machine with a load cell capacity of 0–50 kN (Make: BiSS Microsystems: UT-02-005) where the sample shortens in length with an applied compressive load. The sample changes in diameter and length are found as the cross head of UTM that moves inwards at a constant rate of $6 \times 10^{-4}$ m/s. For each composition, five samples were tested, and the average was considered for the study.

### 2.8 *Impact test*

Impact resistance of the test samples is found as per the ASTM E23 standard with a hammer weight of 150 N (Make: Mechatronic systems: AIT-300-MA). A notched test sample was used to calculate the impact strength and five samples from each composition were tested, and an average value was taken.

### 3 Results and Discussion

### 3.1 *Density and porosity*

The theoretical versus experimental density plot is shown in Figure 5, where the difference in density noted was very minimal comparing between the cast sample and the theoretical value. This variation in

density is due to casting defects and is confirmed by the presence of porosity in the cast sample, which is less than 5% as shown in Figure 6. Shirvanimoghaddam *et al.* were found similar results in that the weight of the hybrid composite reduced with an increase in weight percentage of reinforcements, due to low density of $B_4C$ and Gr [20], [31].

### 3.2 *Hardness test: experimental and statistical effects*

Figure 7(a) depicts the Brinell hardness results for the test samples obtained from the experimental tests. Al7029 alloy hardness value of 67 BHN was found, and a maximum hardness value of 126 BHN was found for sample C3. The increase in hardness was due to an increase in $B_4C$ particle weight percentage and constant wt% of Gr particles [28], [29], [32]–[36]. A linear model built using the statistical tool MINITAB and the regression Equation (1) been developed to evaluate the hardness results obtained experimentally.
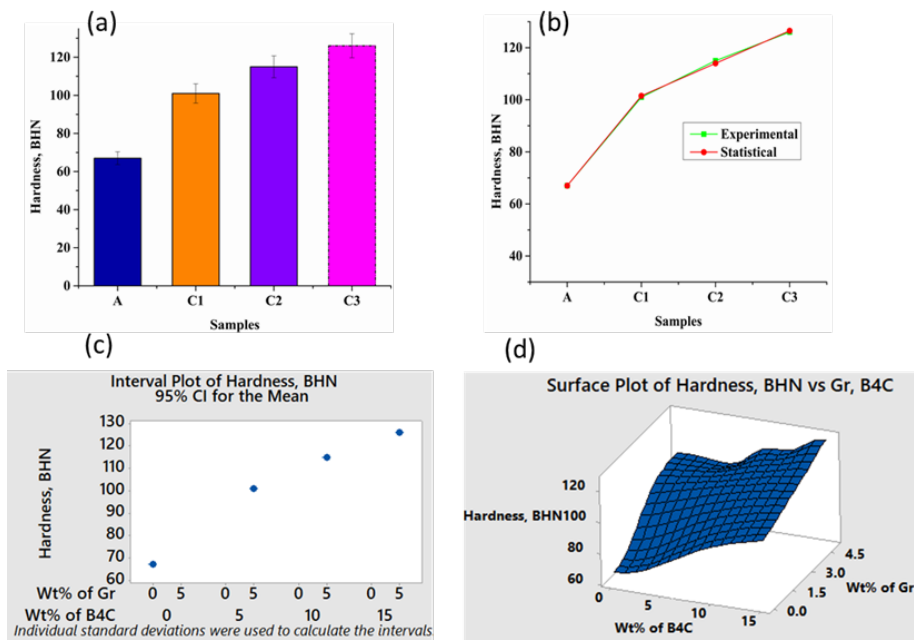
**Table 3**: ANOVA results for Hardness test

| Source | Df | SS | Msq | F-value | P-value | % Contribution |
|---|---|---|---|---|---|---|
| Reg | 2 | 1969.26 | 984.63 | 8960.08 | 0.0078 | - |
| $B_4C$ | 1 | 799.51 | 799.51 | 7275.54 | 0.0072 | 81.19 |
| Gr | 1 | 310.20 | 185.10 | 1684.41 | 0.0017 | 18.81 |
| Error | 1 | 0.11 | 0.11 | | | |
| Total | 3 | 1969.36 | | | | ` |

$R^2$ = 99.92% and Adj. $R^2$ = 99.77%; Df - Degree of freedom; Reg - Regression; SS - Sum of Squares; Msq - Mean Square

$$\text{Hardness} = 67.00 + 2.5^* \text{ wt.\% } B_4C + 4.4^*\text{wt.\% Gr} \tag{1}$$

**Figure 7**: Hardness characteristics, (a) Hardness Value of samples, (b) Error graph, (c) Effect of Reinforcement on Hardness, (d) 3D contour plot.

Figure 7(b) depicts the plots of the experimental and statistical values. The error value found was less than 5%, which confirms the adequacy of the results. From Table 3, it is found that the P-value of the model is 0.0078, which is found to be much less than 0.05 and implies that there is only 0.78% chance of error in the model due to noise. Therefore, the built regression model is very significant. From the literature, it is found that the regression model is reliable if the regression coefficient ($R^2$) exceeds 0.9 [37]. From the regression analysis for the built model, the $R^2$ value is found to be 0.9992. Table 3 also shows that $B_4C$ contributes 81.19% to hardness and Gr contributes 18.81% to hardness. Figure 7(c) depicts the effect of $B_4C$ and Gr weight percent on hardness. The increase in hardness was due to an increase in $B_4C$ particle weight percentage and a constant wt.% of Gr particles. The 3D contour plot shown in Figure 7 (d) confirms that the sample C3 has the highest hardness of all, and that hardness increases with an increase in reinforcement. The constant weight percent of Gr particles reduced the porosity of the composite and the hardness of HMMCs was found to increase with an increase in $B_4C$ particles. The obtained results correlate with the work done by Sharath *et al.* [7] and Subramaniam *et al.* [11].

### 3.3 *Tensile test: experimental and statistical effects*

Figure 8(a) depicts the maximum tensile strength (TS) for test samples obtained from experimental tests using UTM. The Al7029 alloy showed a tensile strength of 180.14 MPa. A maximum TS of 254.121 MPa was found for sample C1. The TS of composites improved up to 10 wt% of reinforcement added and decreased thereafter. However, sample C2 showed an increased strength of 21.44% compared to the base alloy. Material strengthening is observed with the presence of Gr and a greater weight percentage of $B_4C$. Verma *et al.* [21] and Madhu *et al.* [28] were found with similar results for 7-series aluminium alloy.

The fractured surface micrographs of tensile test samples obtained from SEM are shown in Figure 9. As shown in Figure 9 sample A, micro void inclusion caused the formation of a crack and ductile fracture in Al7029 alloy. Similar results are found by Subramaniam *et al.* [11] where the grain boundary is in transgranular form and the addition of ceramic reinforcement leads to brittle fracture. However, the tensile strength of HMMCs was very much higher than the base alloy. Therefore, the failure is due to the
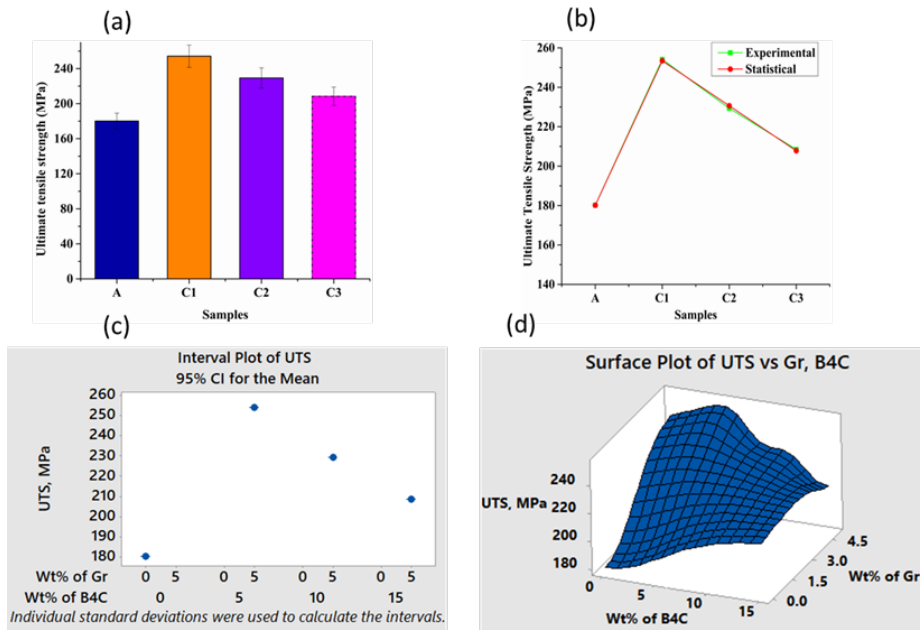
**Figure 8**: Tensile characteristics, (a) Tensile Strength of samples, (b) Error graph, (d) 3D contour plot.

ductile and brittle nature of hybrid composites in samples C1–C3 as shown in Figure 9. HMMCs' resistance to elongation load varies because of the crack initiated and leads to brittle fracture with the propagation of the crack as found to be similar by Gangadhar *et al.* [2].

A linear model built using the statistical tool MINITAB and the regression Equation (2) has been developed to evaluate the tensile strength results obtained experimentally.

$$TS = 180.14 – 4.56* \text{ wt\% } B_4C + 19.23*\text{wt\% Gr} \quad (2)$$

Figure 8(b) depicts the plot of the experimental and statistical values. The error found was less than 5%, which confirms the adequacy of the results. From Table 4, it is found that the P-value of the model is 0.0033, which is found to be much less than 0.05 and implies that there is only a 0.33% chance of error in the model due to noise. Therefore, the built regression model is very significant. From the literature, it is found that the regression model is reliable if the regression coefficient ($R^2$) exceeds 0.9 [37]. From the regression analysis for the built model, the $R^2$ value was found to be 0.9991. Table 4 also shows that $B_4C$ contributes 72.69% and Gr contributes 27.31% to tensile strength.

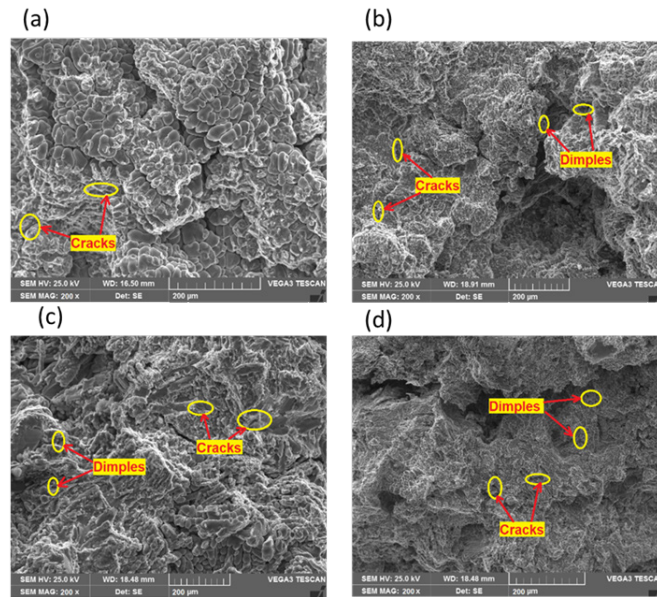**Table 4**: ANOVA results for tensile test of composites

| Source | Df | SS | Msq | F-value | P-value | % Contribution |
|--------|-----|--------|--------|---------|---------|----------------|
| Reg | 2 | 2953.9 | 1476.9 | 2215.5 | 0.003 | - |
| $B_4C$ | 1 | 2772.6 | 2772.5 | 4158.8 | 0.003 | 72.69 |
| Gr | 1 | 1041.3 | 1041.3 | 1561.9 | 0.003 | 27.31 |
| Error | 1 | 0.12 | 0.12 | | | |
| Total | 3 | 2954.1 | | | | |

$R^2$ = 99.91% and Adj. $R^2$ = 99.73%

Figure 8(c) depicts the effect of $B_4C$ and Gr weight percentages on tensile strength. For all other compositions, the tensile strength up to 10% reinforcement was the highest and found to be greater than sample A. The 3D contour plot shown in Figure 8(d) also confirms that the sample C3 has the highest tensile strength. The tensile strength of HMMCs is reduced after 15 wt% of reinforcement due to the brittle nature of the material [2], [38].

**3.4 Compression test: experimental and statistical effects**

The compressive characteristics for test samples obtained from an experimental test using UTM are as shown in Figure 10(a). Sample A showed a compressive strength (CS) of 346.205 MPa. The maximum CS

**Figure 9**: Tensile fractured samples micrographs,(a) Sample A, (b) Sample C1, (c) Sample C2, (d) Sample C3.

of 586.841 MPa was found in sample C3. A linear model built using the statistical tool MINITAB and the regression Equation (3) was developed to evaluate the compression strength results obtained experimentally.

$$CS = 346.20 + 14.51* \text{wt\% } B_4C + 4.39*\text{wt\% Gr} \quad (3)$$

**Table 5**: ANOVA results for Compressive test

| Source | Df | SS | Msq | F-value | P-value | % Contribution |
|--------|-----|---------|---------|---------|---------|----------------|
| Reg | 2 | 5143.14 | 2571.57 | 3625.91 | 0.0041 | - |
| B$_4$C | 1 | 1985.24 | 1985.24 | 2799.18 | 0.0083 | 77.23 |
| Gr | 1 | 585.14 | 585.14 | 825.04 | 0.050 | 22.77 |
| Error | 1 | 0.13 | 0.13 | | | |
| Total | 3 | 5143.27 | | | | |

R$^2$ = 99.99% and Adj. R$^2$ = 99.97%

From Table 5, it is found that the P-value of the model is 0.05, which is found to be a significant value and implies that there exists only a 5% chance of error in the model due to noise. Therefore, the built regression model is significant. From the literature, it is found that the regression model is reliable if the regression coefficient (R$^2$) exceeds 0.9 [37]. From the regression analysis for the built model, the R$^2$ value was found to be 0.9999. Table 5 also shows that B$_4$C contributes 77.23% to CS, while Gr contributes 22.77%. The effect of B$_4$C and Gr weight percentages on compressive strength is shown in Figure 10(c).

The increase in compressive nature was due to an increase in B$_4$C particle weight percentage and constant wt% of Gr particles. The 3D contour plot shown in Figure 10(d) confirms that the sample C3 has the highest strength of all and that CS increased with an increase in reinforcement. Results obtained by Kuldeep *et al.* and Verma *et al.* were similar where the constant weight percent of Gr particles reduced the porosity of the composite and the compressive strength of HMMCs was found to increase with an increase in B$_4$C particles [13], [21].

### 3.5  *Impact test: experimental and statistical effects*

Figure 11(a) depicts the impact characteristics of test samples obtained from experimental tests. Sample A has an impact energy (IE) of 2 J. The maximum IE of 7 J was found for sample C1. The IE of composites improved up to 10wt.% of reinforcement added and decreased thereafter. However, sample C2 showed an increased impact strength of 66.66% more than sample A. Material strengthening is observed with the presence of Gr and a greater weight percentage of B$_4$C [28].

The fractured surface micrographs of impact test samples obtained from SEM are shown in Figure 12. Figure 12(a) depicts the formation of a crack and
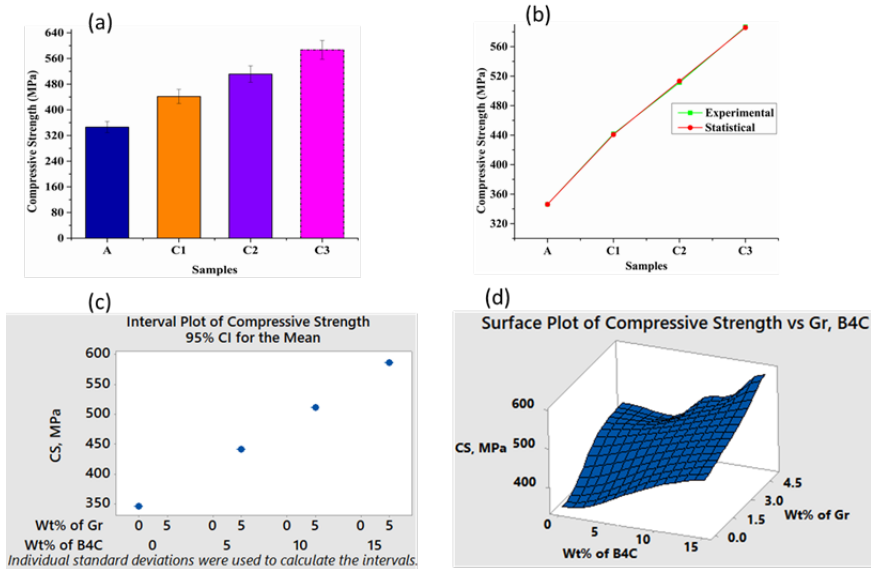
**Figure 10**: Compressive characteristics, (a) Compressive Strength of samples, (b) Error graph, (c) Effect of Reinforcement on Compressive Strength, (d) 3D contour plot.
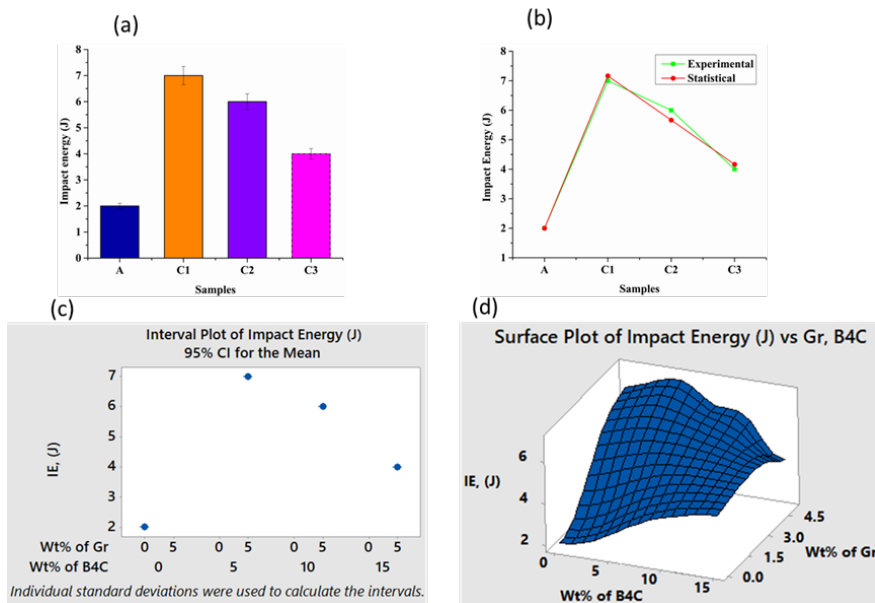


**Figure 11**: Impact characteristics, (a) Impact Strength of samples, (b) Error graph, (c) Effect of Reinforcement on Impact Strength, (d) 3D contour plot.

ductile fracture in sample A as a result of micro void inclusion. The brittle fracture was observed in the highly stressed region that initiated the crack, and particle clustering was not observed due to the uniform distribution shown in Figure 12(b)–(d).

The impact strength of HMMCs was very much higher than that of the base alloy. $B_4C$ and Gr particles act as barriers to dislocation. Impact energy increased with better bonding between particles. Trans granular cleavages and intergranular cracks lead to brittle fracture
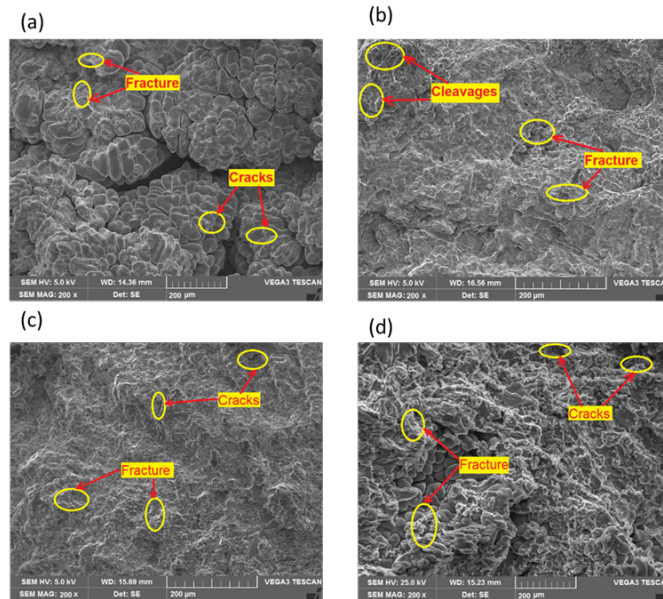
**Figure 12**: Impact fractured micrographs: (a) Sample A, (b) Sample C1, (c) Sample C2, (d) Sample C3.

[11], [38]. A linear model built using the statistical tool MINITAB and the regression Equation (4) was developed to evaluate the tensile strength results obtained experimentally.

$$IE = 2 - 0.30 * wt\% \ B_4C + 1.333 * wt\% \ Gr \qquad (4)$$

Figure 11(b) depicts the plot of the experimental and statistical values. The error found was less than 5%, which confirms the adequacy of the results.

**Table 6**: ANOVA results for Impact test

| Source | Df | SS | Msq | F-value | P-value | % Contribution |
|--------|----|------|------|---------|---------|----------------|
| Reg | 2 | 22.6 | 11.3 | 94.7 | 0.0076 | - |
| $B_4C$ | 1 | 15.9 | 15.9 | 133.9 | 0.0084 | 76.59 |
| Gr | 1 | 4.9 | 4.87 | 40.9 | 0.0044 | 23.41 |
| Error | 1 | 0.09 | 0.09 | | | |
| Total | 3 | 22.7 | | | | |

$R^2$ = 99.41% and Adj. $R^2$ = 98.23%

From Table 6, it is found that the P-value of the model is 0.0084, which is found to be equal to a significant value and implies that there is only 0.84% chance of error in the model due to noise.

Therefore, the built regression model is significant. From the literature, it is found that the regression model is reliable, if the regression coefficient ($R^2$) exceeds 0.9 [31]. From the regression analysis for the built model, the $R^2$ value was found to be 0.9941. Table 6 also shows that $B_4C$ contributes 76.59% of the total impact energy, while Gr contributes 23.41%.

Figure 11(c) depicts the effect of $B_4C$ and Gr weight percentages on impact strength. The impact strength up to 10 wt% of reinforcement was the highest and found to be more than sample A. The 3D contour plot shown in Figure 11(d) also confirms that the sample C1 has the highest impact strength. Results obtained by Gangadhar *et al.* and Kuldeep *et al.* were similar where the impact strength of HMMCs was reduced after 15 wt% of reinforcement due to the increased brittle nature of the material [2], [13].

## 4 Conclusions

Hybrid Al7029/$B_4$C/Gr composites were successfully fabricated using the stir casting route. The hybrid composites were evaluated for mechanical behavior by experimental and statistical studies, which concluded that uniform particle ($B_4C$ and Gr) distribution within the matrix (Al7029) was confirmed by SEM analysis. XRD analysis confirms that there is no additional phase change in HMMCs. The porosity of cast samples was minimal and found to decrease from sample

A1 to C2, whereas in sample C3, porosity increased due to particle agglomeration at a higher wt% of reinforcement. The weight of hybrid composites is reduced due to the low density of $B_4C$ and Gr compared to Al7029 alloy. The hardness and compressive strength of the hybrid composite increased because the reinforcement was evenly distributed and there was a strong bond between the matrix and the reinforcement. The reinforcements ($B_4C$ and Gr) added to the Al7029 matrix increased tensile and impact strength for all compositions compared to the Al7029 alloy. Tensile and impact strength of the hybrid composite increased up to 10 wt% of reinforcement. Further, the decrease in energy absorption capacity is due to cracks and micro pores formed. Fractured SEM micrographs justify that $B_4C$ and Gr act as barriers to dislocation within the matrix and absorb energy due to their high fracture toughness. The experimental and statistical results are in good agreement with each other with nominal error. The addition of $B_4C$ and Gr improved mechanical properties, and the Al7029/ 10 wt%$B_4C$/5 wt%Gr hybrid composite (sample C2 with a hardness of 41%, a tensile strength of 22%, a compressive strength of 32%, and an impact strength of 60% more than the base alloy) could be the best composite suited for aerospace and automotive structural applications. Future plans for the work can be extended to check the tribological suitability of hybrid composites.

## References

[1] T. Dursun and C. Soutis, "Recent developments in advanced aircraft aluminium alloys," *Materials & Design*, vol. 56, pp. 862–871, Apr. 2014, doi: 10.1016/j.matdes.2013.12.002.

[2] T. G. Gangadhar, D. P. Girish, J. Satheesh, H. Govtham, and K. S. Pradeep, "Evaluation of mechanical properties of Al7029/flyash/WC hybrid composites developed by liquid metallurgy," in *Materials Today: Proceedings*, 2021, pp. 5969–5974, doi: 10.1016/j.matpr.2020.12.401.

[3] H. Kala, K. K. S. Mer, and S. Kumar, "A review on mechanical and tribological behaviors of stir cast aluminum matrix composites," in *Procedia Materials Science*, 2014, pp. 1951–1960, doi: 10.1016/j.mspro.2014.07.229.

[4] A. H. Jasim, W. M. Joudi, N. S. Radhi, and A. N. Saud, "Mechanical properties and wear characteristic of (Aluminum-Zinc oxide) metal matrix composite prepared using stir casting process," in *Materials Science Forum*, 2020, pp. 175–184, doi: 10.4028/www.scientific.net/MSF.1002.175.

[5] M. Tisza and Z. Lukács, "High strength aluminum alloys in car manufacturing," in *IOP Conference Series: Materials Science and Engineering*, 2018, Art. no. 012033, doi: 10.1088/1757-899X/418/1/012033.

[6] M. K. Surappa and P. K. Rohatgi, "Preparation and properties of cast aluminium-ceramic particle composites," *Journal of Materials Science*, vol. 16, no. 4, pp. 983–993, Apr. 1981, doi: 10.1007/ BF00542743.

[7] B. N. Sharath, K. S. Madhu, and C. V. Venkatesh, "Experimental study on dry sliding wear behaviour of Al-B4C-Gr metal matrix composite at different temperatures," in *Applied Mechanics and Materials*, 2019, pp. 96–101, doi: 10.4028/www.scientific. net/AMM.895.96.

[8] B. N. Sharath, C. V. Venkatesh, A. Afzal, N. Aslfattahi, A. Aabid, M. Baig and B. Saleh, "Multi ceramic particles inclusion in the aluminium matrix and wear characterization through experimental and response surface-artificial neural networks," *Materials*, vol. 14, no. 11, May. 2021, Art. no. 2895, doi: 10.3390/ma14112895.

[9] B. N. Sharath, T. P. Jeevan, M. A. A. Baig, H. S. Ashrith, A. Afzal, and A. Raji Reddy, "Machinability studies on boron carbide and graphite reinforced aluminium hybrid composites," in *Materials Today: Proceedings*, 2021, pp. 8734– 8741, doi: 10.1016/j.matpr.2021.04.036.

[10] B. N. Sharath and C. V. Venkatesh, "Study on effect of boron carbide, aluminium oxide and graphite on dry sliding wear behaviour of aluminium based metal matrix composite at different temperature," *Tribologia - Finnish Journal of Tribology*, vol. 38, no. 1−2, pp. 35–46, Jun. 2021, doi: 10.30678/fjt.99931.

[11] B. Subramaniam, B. Natarajan, B. Kaliyaperumal, and S. J. S. Chelladurai, "Investigation on mechanical properties of aluminium 7075 - boron carbide - coconut shell fly ash reinforced hybrid metal matrix composites," *China Foundry*, vol. 15, no. 6, pp. 449–456, Nov. 2018, doi: 10.1007/ s41230-018-8105-3.

[12] P. R. Jadhav, B. R. Sridhar, M. Nagaral, and J. I. Harti, "Mechanical behavior and fractography of graphite and boron carbide particulates reinforced A356 alloy hybrid metal matrix composites," *Advanced Composites and Hybrid Materials*, vol. 3, no. 1, pp. 114–119, Mar. 2020, doi: 10.1007/s42114-020-00143-7.

[13] B. Kuldeep, K. P. Ravikumar, S. Pradeep, and K. R. Gopi, "Effect of boron nitride and zirconium dioxide on mechanical behavior of Al7075 metal matrix hybrid composite," *Materials Research Express*, vol. 6, no. 3, Dec. 2018, Art. no. 036509, doi: 10.1088/2053-1591/aaf36b.

[14] M. V. Krishna and A. M. Xavior, "An investigation on the mechanical properties of hybrid metal matrix composites," in *Procedia Engineering*, 2014, pp. 918–924, doi: 10.1016/j.proeng.2014.12.367.

[15] G. Senthilkumar, T. Mayavan, and R. Ramakrishnan, "Optimization for friction welding input factors to maximize tensile strength and minimize axial shortening in ASTM A516 grade 70 steel rods," *Journal of Applied Science and Engineering*, vol 25, no. 5, pp. 773–784, Dec. 2021, doi: 10.6180/jase.202210_25(5).0008.

[16] P. Kongkaoroptham, M. Boonpensin, T. Siripongsakul, and P. Promdirek, "Corrosion Behaviour of AISI409 Stainless Steel with Al Slurry Coating in Molten Salt," *Applied Science and Engineering Progress*, vol. 15, no. 1, Feb. 2021, Art. no. 3523, doi: 10.14416/j.asep.2021.02.002.

[17] P. S. Reddy, R. Kesavan, and B. Vijaya Ramnath, "Investigation of mechanical properties of aluminium 6061-silicon carbide, boron carbide metal matrix composite," *Silicon*, vol. 10, no. 2, pp. 495–502, Jan. 2017, doi: 10.1007/s12633-016-9479-8.

[18] Y. L. Chan, K. Y. You, M. Z. H. Mayzan, M. A. Jusoh, Z. Abbas, and F. Esa, "Investigation into return loss characteristic of graphene oxide/zinc ferrite/epoxy composite at x-band frequency," *Journal of Applied Science and Engineering*, vol 23, no. 4, pp. 593–602, Jul. 2020, doi: 10.6180/jase.202012¬_23(4).0003.

[19] K. Jayappa, V. Kumar, and G. G. Purushotham, "Effect of reinforcements on mechanical properties of nickel alloy hybrid metal matrix composites processed by sand mold technique,"

*Applied Science and Engineering Progress*, vol 14, no. 1, pp. 44–51, Jan. 2021, doi: 10.14416/j.asep.2020.11.001.

[20] K. Shirvanimoghaddam, H. Khayyam, H. Abdizadeh, M. K. Akbari, A. H. Pakseresht, E. Ghasali, and M. Naebe, "Boron carbide reinforced aluminium matrix composite: Physical, mechanical characterization and mathematical modelling," *Materials Science and Engineering: A*, vol. 658, pp. 135–149, Mar. 2016, doi: 10.1016/j.msea.2016.01.114.

[21] N. Verma and S. C. Vettivel, "Characterization and experimental analysis of boron carbide and rice husk ash reinforced AA7075 aluminium alloy hybrid composite," *Journal of Alloys and Compounds*, vol. 741, pp. 981–998, Apr. 2018, doi: 10.1016/j.jallcom.2018.01.185.

[22] V. Mohanavel, K. Rajan, S. S. Kumar, G. Vijayan, and M. S. Vijayanand, "Study on mechanical properties of graphite particulates reinforced aluminium matrix composite fabricated by stir casting technique," in *Materials Today: Proceedings*, 2018, pp. 2945–2950, doi: 10.1016/j.matpr.2018.01.090.

[23] T. H. Manjunatha, Y. Basavaraj, M. Nagaral, V. Venkataramana, and J. I. Harti, "Investigations on mechanical behavior of Al7075 - nano B4C composites," in *IOP Conference Series: Materials Science and Engineering*, 2018, Art. no. 012091, doi: 10.1088/1757-899X/376/1/012091.

[24] İ. ŞİMŞEK, "The effect of B4C amount on wear behaviors of Al-Graphite/B4C hybrid composites produced by mechanical alloying," *Journal of Boron*, vol. 4, no. 2, pp. 100–106, Jun. 2019, doi: 10.30728/boron.556707.

[25] X. Lyu, Z. Zhao, H. Sun, X. Jiang, C. Hu, T. Song, and Z. Luo, "Influence of $Y_2O_3$ contents on sintering and mechanical properties of $B_4C$-$Al_2O_3$ multiphase ceramic composites," *Journal of Materials Research and Technology*, vol. 9, no. 5, pp. 11687–11701, Sep. 2020, doi: 10.1016/j.jmrt.2020.08.072.

[26] B. N. Sharath, C. V. Venkatesh, A. Afzal, M. A. A. Baig, and A. P. Kumar, "Study on effect of ceramics on dry sliding wear behaviour of Al-Cu-Mg based metal matrix composite at different temperature," in *Materials Today: Proceedings*, 2021, pp. 8723–8733, doi:

10.1016/j.matpr.2021.04.034.

[27] D. G. Pradeep, B. N. Sharath, A. Afzal, M. A. A. Baig, and M. Shanmugasundaram, "Study on scratch behavior of Ni-Al$_2$O$_3$ coating composition on Al-2219 substrate by electro deposited technique," in *Materials Today: Proceedings*, 2021, pp. 8716–8722, doi: 10.1016/j.matpr. 2021.04.033.

[28] K. S. Madhu, B. N. Sharath, C. V. Venkatesh, and D. G. Pradeep, "Evaluation of mechanical properties of ceramic reinforced aluminium-7029 hybrid composite," in *IOP Conference Series: Materials Science and Engineering*, 2021, Art. no. 012019, doi: 10.1088/1757-899X/1189/1/012019.

[29] B. N. Sharath, K. S. Madhu, D. G. Pradeep, and C. V. Venkatesh, "Tribological suitability of aluminium hybrid composite above atmospheric temperature," in *IOP Conference Series: Materials Science and Engineering*, 2021, Art. no. 012018, doi: 10.1088/1757-899X/1189/1/012018.

[30] D. G. Pradeep, H. S. Nithin, B. N. Sharath, K. S. Madhu, and C.V. Venkatesh, "Microstructure and wear behavior of microwave treated WC-10Co-4Cr composite coating on AISI 4140 alloy steel," in *IOP Conference Series: Materials Science and Engineering*, 2021, Art. no. 012012, doi: 10.1088/1757-899X/1189/1/012012.

[31] K. S. Madhu, C. V. Venkatesh, B. N. Sharath, and S. Karthik, "Effect of boron carbide on wear resistance of graphite containing Al7029 based hybrid composites and its dry sliding wear characterization through experimental, response surface method and ANOVA," *Tribologia - Finnish Journal of Tribology*, vol. 38, no. 3−4, pp. 48–60, Dec. 2021, doi: 10.30678%2Ffjt.1119.

[32] A. Bahrami, N. Soltani, M. I. Pech-Canul, S. Soltani, L. A. González, C. A. Gutiérrez, J. Tapp, A. Moller, and A. Gurlo, "Bilayer graded Al/B$_4$C/rice husk ash composite: Wettability behavior, thermo-mechanical, and electrical properties," *Journal of Composite Materials*, vol. 52, no. 27, pp. 3745–3758, Nov. 2018, doi: 10.1177%2F0021998318769993.

[33] A. Bahrami, M. I. Pech-Canul, N. Soltani, C. A. Gutiérrez, P. H. Kamm, and A. Gurlo, "Tailoring microstructure and properties of bilayer-graded Al/B$_4$C/MgAl$_2$O$_4$ composites by single-stage pressureless infiltration," *Journal of Alloys and Compounds*, vol. 694, pp. 408–418, Feb. 2017, doi: 10.1016/j.jallcom.2016.09.284.

[34] S. D. Kumar, M. Ravichandran, A. Jeevika, B. Stalin, C. Kailasanathan and A. Karthick, "Effect of ZrB$_2$ on microstructural, mechanical and corrosion behaviour of aluminium (AA7178) alloy matrix composite prepared by the stir casting route," *Ceramics International*, vol. 47, no. 9, pp. 12951–12962, May. 2021, doi: 10.1016/j.ceramint.2021.01.158.

[35] B. Stalin, P. R. Kumar, M. Ravichandran, and S. Saravanan, "Optimization of wear parameters and their relative effects on stir cast AA6063-Si$_3$N$_4$ composite," *Materials Research Express*, vol. 5, no. 10, Aug. 2018, Art. no. 106502, doi: 10.1088/2053-1591/aad99c.

[36] J. Vairamuthu, B. Stalin, G. D. Sivakumar, B. M. Fazil, R. Balaji and V. A. Natarajan, "The effect of process parameters for synthesized copper metal matrix using stir casting process," in *Materials Today: Proceedings*, 2021, pp. 1970–1974, doi: 10.1016/j.matpr.2020.09.262.

[37] S. Ramasamy, A. Arumugam, and P. Chandran, "Optimization of enterobacter cloacae (KU923381) for diesel oil degradation using response surface methodology (RSM)," *Journal of Microbiology*, vol. 55, no. 2, pp. 104–111, Jan. 2017, doi: 10.1007/s12275-017-6265-2.

[38] P. P. Ritapure and Y. R. Kharde, "Study of mechanical and sliding wear behavior of Al-25Zn alloy/SiC/Graphite novel hybrid composites for plain bearing application," *Tribology in Industry*, vol. 41, no. 3, pp. 375–386, Sep. 2019, doi: 10.24874/ti.2019.41.03.07.